FERMILAB-LU-105

F. Mills, RFQ talk 11/3/1987

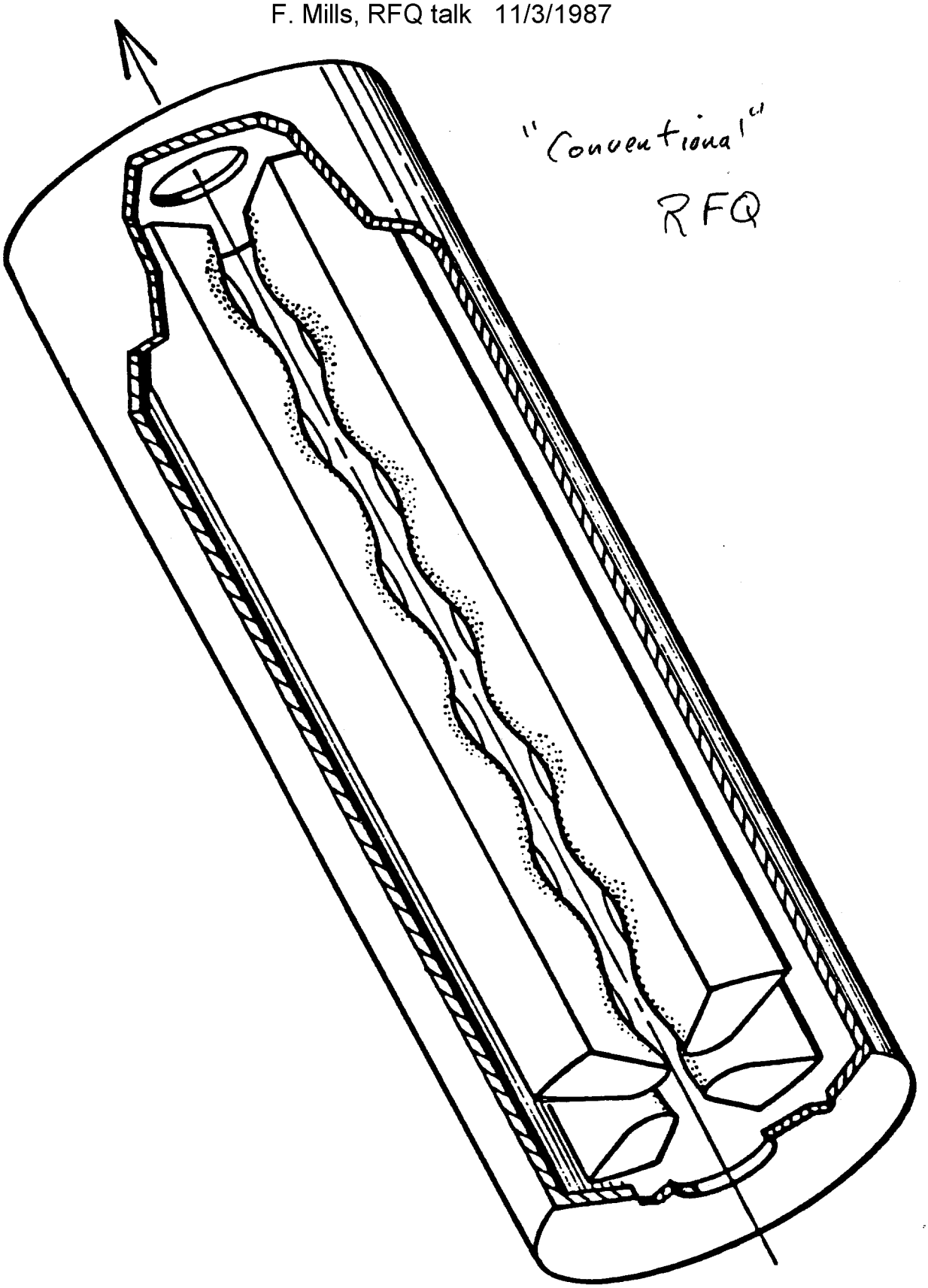

Startup of the URAL-15 linear proton accelerator with quadrupole rf focusing

B. M. Gorshkov, S. A. Il'evskii, G. M. Kolomenskii, S. P. Kuznetsov, N. N. Kutorga, A. P. Mal'tsev, I. G. Mal'tsev, K. G. Mirzoev, V. B. Stepanov, V. A. Teplyakov, and I. M. Shalashov

Institute of High-Energy Physics, Protvino

(Submitted September 28, 1976)

Zh. Tekh. Fiz. 47, 2328–2331 (November 1977)

The URAL-15 accelerator is the first stage of a 30 MeV linear accelerator (the URAL-30), intended for use as an injector into the booster of the proton synchrotron of the Institute of High-Energy Physics. The basic parameters of the accelerator and the results of the first startup and adjustment experiments are reported. Accelerated protons with an energy of 15.9 MeV have been obtained. The maximum accelerated current is greater than 50 mA. The spectral width of the pulses is 1.2%. The normalized emittance is less than 0.3 mrad-cm.

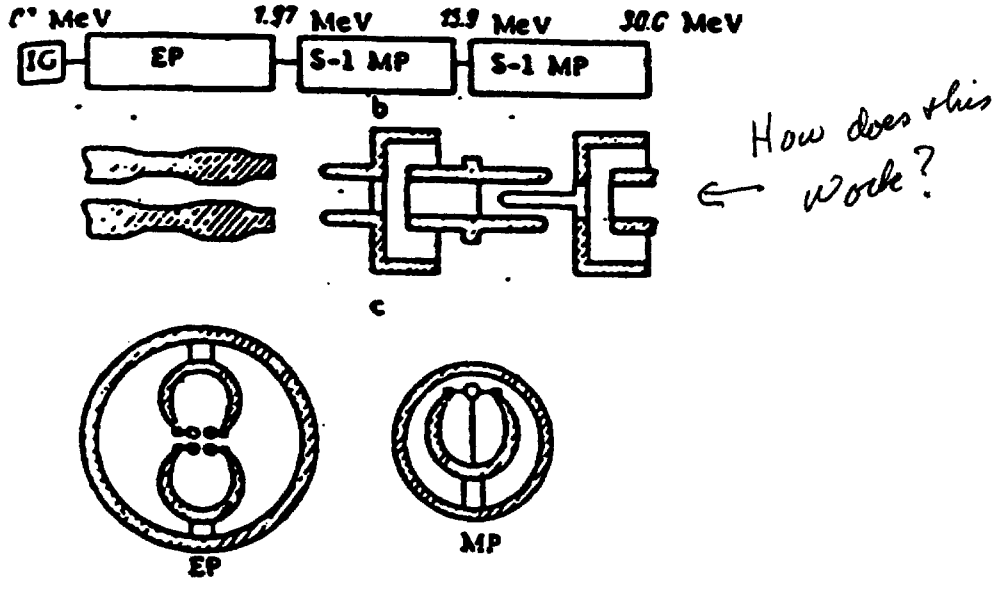

FIG. 1. a) Block diagram of the URAL-30 accelerator; b) electrode shape; c) resonator cross sections.

Parameter	EP	MP
Injection energy, MeV	0.1	1.97
Output energy, MeV	1.97	15.9
Design accelerated current, mA	130	100
Spectral width of pulses (at base), %	±3.2	±1.2
Normalized emittance, mrad·cm	0.5–1	0.5–1
Current pulse length, μsec	10	10
Repetition frequency of the pulses in packet, Hz	25	25
Repetition frequency of the packets, Hz	0.2	0.2
Steady-state oscillator power, MW	1.5	4.5
Working frequency, MHz	148.5	148.5
Container length, m	3.5	6.7
Container diameter, m	0.52	0.4

Helmholtz Equations

$(A, \Psi)\, e^{i\omega t}$

$\nabla^2 A + k_0^2 A = 0$

$\nabla^2 \Psi + k_0^2 \Psi = 0$

$k_0 = \omega / c$

Quasistatic Approximation

$\Psi e^{i\omega t}$

$\nabla^2 \Psi = 0 \quad \Psi \rightarrow R_{km}(r) e^{i(\pm kz \pm m\phi)}$

OK when $k_0 \ll k$

"Conventional" RFQ uses only two terms, and then one calculates the pole profile.

Rod Type – specify profile, calculate effects of many terms. (A la Schempp)

INVESTIGATIONS OF DIFFERENT RFQ ELECTRODE PROFILES FOR EASY MANUFACTURE*

P. Junior, H. Deitinghoff, A. Harth, W. Neumann, N. Zoubek
Institut für Angewandte Physik, University Frankfurt
Robert-Mayer-Straße 2-4, 6000 Frankfurt am Main, FRG

Abstract

Four electrode profiles are analyzed with respect to field harmonics in the three-dimensional potential caused by profiles, which deviate from the ideal one. Emphasis is given to such electrodes, which can easily be manufactured on a conventional milling machine or a lathe.

The following versions are discussed: 1) the "crankshaft" type, 2) the barrel profile, 3) the trapezoidal electrodes, 4) the finger structure.

Our computational method in calculating the momenta is reported. Finally the influence of relevant coefficients in the potential expansion on particle motion is examplarily studied by means of a 10 - 300 keV proton RFQ linac.

RFQ Profiles

Conventional RFQ linac designs are based on the two term potential[1]. But this involves particular demands on the electrodes. An example was set by the Los Alamos POP experiment[2], where the manufacture of approximately ideal electrodes was accomplished with a computerized milling machine. However, the request for an easier construction becomes obvious. Figs. 1 show principles requiring tools more moderate and in consideration of this the following configurations shall be discussed.

1. The crankshaft structure of figs. 1a, 1b and 2 with constant bore radius $R_1 = R_2$ and rectangularly varying distance R_X resp. R_Y.
2. The cylindrical barrels of figs. 1a, 1b and 3 with constant distance $R_X = R_Y$ and rectangularly varying bores R_1 resp. R_2.
3. Cylindrical rods with constant distance $R_X = R_Y$ and trapeziodally varying bore, as figs. 1a, 1c and 4 illustrate. The principle is realized with $\vartheta = 0.75$ in our proton linac[3,4,5]
4. The fingers with gaps in between, constant bore $R_1 = R_2$ as well as distance $R_X = R_Y$ according to figs. 1a, 1d. This scheme is realized in the GSI MAXILAC[6].

Deviations from the ideal two term case are obvious, thus the performance of higher field moments is the aim of investigations.

3-D Computations

Use is made of the expansion of the potential[1]

$$\Psi(r,\phi,z) = \frac{V}{2} \sum_{\substack{M=0 \\ N=0}}^{\infty} A_{NM} F_{NM}(r,\phi,z) \qquad (1)$$

with

$$F_{NM} = \begin{cases} r^{2M}\cos 2M\phi & N = 0 \\ I_{2M}(Nkr)\cos 2M\phi \cos Nkz & N \geq 1 \end{cases} \qquad (2)$$

and for the determination of the coefficients A_{NM} at given electrode geometry we have composed a computer program. It is based on a three-dimensional least square fit of eq. (1) to the spatial electrode surface. Considering all L relevant coefficients $A_{NM} = X_I$ in arbitrary sequence I = 0...L-1, those are gained as solutions of an inhomogeneous system of L linear equations

$$\sum_{K=0}^{L-1} H_{IK} X_I = R_I \qquad (3)$$

where with eq. (2) the matrix elements are given by surface integrals

$$H_{IK} = \iint I_{IM} \cdot F_{NK}\, r\,d\phi\,dz$$
$$R_I = \iint F_{NM}\, r\,d\phi\,dz \qquad (4)$$

extended over the surface $r = r(\phi,z)$ of the electrodes. According to RFQ symmetry the axial range is only $\pi/2$ and all A_{NM} vanish, when N+M even. Boundary conditions yet undefined in the gap PQ (fig. 1a) are settled by an assumed two-wire potential here. The reliability of results, e. g. what this approximation is concerned, is always checked with the agreement to the voltage on the electrodes, for a precision of about 1 % the order L = 30 of eqs. (3) is mostly required.

Results

Referring to our linac[3,4,5] figs. 5 demonstrate relevant field harmonics occuring with the electrodes 1 - 3 together with the two term coefficients and it's approximation by a harmonic modulation, which can be realized with a milling wheel of constant curvature, however, the increasing cell length in the linac complicates manufacture as well. We have singled out as a representative section the last one at 300 keV. As striking evidence we state that a significant gain in acceleration rate A_{10} compared to the rate with ideal $A_{10}{}^{I}$ at nearly unchanged focusing strength A_{01} takes place in all our cases, however, accompanied by an additive quadrupole term A_{21} and an octupole term A_{12}. Dodekapoles A_{03} and A_{23} turn out too small in all cases to influence particle motion. Neither does jittering caused by A_{30} play a role. Effects on linear motion characterized by the behaviour of the transverse phase advance per period are illustrated in fig. 6. At given transverse phase advance the acceleration rate is more or less significantly improved with all configurations 1 - 3, when compared to the ideal electrode or it's harmonic approximation. This is partially caused by the quadrupole term A_{21} proving helpful when negative. Effects are illustrated by fig. 7, where a particle beam of 10 mA is traced through the linac. The plot shows gains and losses due to A_{21} and A_{12} either in- or excluded , effects seem negligible . It seems that in all our cases the higher momenta are too small to have any negative effect on particle motion, although they usually are not too small for the proper evaluation of all coefficients. Here we can state that for proton linacs admitting large transverse phase advances the ideal surface profile has the disadvantage in construction as well as in acceleration rate at given phase advances. The behaviour of the fingers (s. fig. 1d) is illustrated in fig. 8, where the gap is varied. Together with a strong A_{01} an impressive negative A_{21} term shows up. Now the consequence is that a strong overfocusing happens with our proton data of fig. 6, however, when we consider a typical situation with very heavy ions[6] quite favourable transverse phase advances occur with this structure. Present work is concerned with effects in heavy ion acceleration using all these electrodes, when low charge states demand operation much nearer to the stability limits. Then of course the knowledge of the A_{NM} will be utilized for the determination of peak surface fields.

Computations were carried out at the Hochschulrechenzentrum.

References

1 I.M. Kapchinskij, V.A. Treplyakov, Prob. Tekh. Eksp. No. 2 (1969) 19
2 R.W. Hamm et al., Int. Conf. on Low Energy Ion Beams 2, Bath, England April 14 - 17, 1980
3 A. Schempp et al., IEEE Trans. Nucl. Sci. NS-30 (1983) p. 3536

* Work supported by BMFT

K. R. Crandall, R. S. Mills, and T. P. Wangler, AT-1, MS H817
Los Alamos National Laboratory, Los Alamos, NM 87545

Summary

Radio-frequency quadrupole (RFQ) linacs[1,2] are becoming widely accepted in the accelerator community. They have the remarkable capability of simultaneously bunching low-energy ion beams and accelerating them to energies at which conventional accelerators can be used, accomplishing this with high-transmission efficiencies and low-emittance growths. The electric fields, used for radial focusing, bunching, and accelerating, are determined by the geometry of the vane tips. The choice of the best vane-tip geometry depends on considerations such as the peak surface electric field, per cent of higher multipole components, and ease of machining.

We review the vane-tip geometry based on the "ideal" two-term potential function and briefly describe a method for calculating the electric field components in an RFQ cell with arbitrary vane-tip geometry. We describe five basic geometries and use the prototype RFQ design for the Fusion Materials Irradiation Test (FMIT) accelerator as an example to compare the characteristics of the various geometries.

Vane-Tip Geometry from Two-Term Potential Function

As a starting point for obtaining electric fields and vane-tip geometry in RFQ linacs, we take

$$U(r,\theta,z) = \frac{V}{2}\left[\left(\frac{r}{r_o}\right)^2 \cos 2\theta + A\, I_o(kr) \cos kz\right] \quad (1)$$

as the time-independent portion of the two-term potential (TTP) function.[3] In this expression, V is the intervane potential difference, and $k = \pi/L$, where $L = \beta\lambda/2$ is the length of one "cell" of the RFQ. Although the cell length and other geometrical characteristics change gradually throughout the linac, the field analysis is done as if each cell were one element in a completely periodic structure.

Let $z = 0$ at the beginning of a cell in which the horizontal vanes (centered at $\theta = 0$) are at the minimum displacement, a, from the z axis; $z = L$ at the end of the cell where the horizontal vane-tip displacement is ma, and m, the modulation parameter, is ≥ 1. The boundary conditions

$$U(a,0,0) = U(ma,0,L) = V/2$$

are used for calculating A and r_o from Eq. (1):

$$A = \frac{m^2 - 1}{m^2 I_o(ka) + I_o(mka)} \quad ; \quad (2)$$

$$r_o = a[1 - A\, I_o(ka)]^{-1/2} \quad . \quad (3)$$

If a and m are specified, A and r_o can be calculated directly. However, because focusing and acceleration depend upon r_o and A, these quantities usually are determined by beam-dynamics requirements, and a and m are calculated by iterating Eqs. (2) and (3).

*Work supported by the US Department of Energy.

Ideally, vane-tip geometries should correspond to the $\pm V/2$ isopotential surfaces obtained from Eq. (1). The longitudinal profile of the horizontal vane tip is denoted by $x_p(z)$ and is found numerically from

$$\left(\frac{x_p}{r_o}\right)^2 + A\, I_o(kx_p) \cos kz = 1 \quad . \quad (4)$$

The transverse radius of curvature at any x_p is

$$\rho_t = x_p\left(\frac{2x_p/r_o + Q}{2x_p/r_o - Q}\right) \quad , \quad (5)$$

where

$$Q = A\, kr_o\, I_1(kx_p) \cos kz \quad .$$

Note that, at the center of the cell where $\cos kz = 0$, both x_p and ρ_t are equal to r_o. The property $x_p = r_o$ at $z = L/2$ is taken as the fundamental definition of r_o for all vane-tip geometries discussed in this paper.

At any longitudinal position, the transverse cross sections of the isopotential surfaces from Eq. (1) are approximate hyperbolae. In practice, the vane tips cannot conform exactly to these shapes because adjacent vanes would approach each other asymptotically, and the surface electric field would increase indefinitely. Also, hyperbolic surfaces are more difficult to machine than circular cross sections. For these reasons, RFQ vane tips have been machined with circular arcs. The earlier versions machined at Los Alamos had longitudinal profiles agreeing with Eq. (4) and circular tips with radii given by Eq. (5).

Calculation of Fields for Arbitrary Geometries

For arbitrary vane-tip geometries, including the geometry described in the previous section, one needs a reliable method for calculating the surface electric field. Our approach to this problem has been to find a good approximation for the charge density induced on the vane-tip surfaces and then to derive the field information from the charge density. For example, the electric field at any point on the vane-tip surface is directly proportional to the charge density at that point; the intervane capacitance is proportional to the total charge on a vane tip. The potential near the vane tips can be calculated from the charge density and can be Fourier analyzed to determine the amplitude of any multipole component.

Written in terms of the surface charge density σ, the potential at any point $\vec{r}$ near the vane tips is

$$U(\vec{r}) = \int G(\vec{r};\vec{s})\, \sigma(\vec{s})\, dS \quad , \quad (6)$$

where $G(\vec{r};\vec{s})$ is the potential produced at point $\vec{r}$ by a unit charge located at point $\vec{s}$ on a vane-tip surface; $\sigma(\vec{s})\, dS$ is the amount of charge in the infinitesimal

R. H. Stokes, K. R. Crandall, J. E. Stovall, and D. A. Swenson

Los Alamos Scientific Laboratory
University of California
Los Alamos, New Mexico 87545

Summary

A method has been developed to analyze the beam dynamics of the radio frequency quadrupole accelerating structure. Calculations show that this structure can accept a dc beam at low velocity, bunch it with high capture efficiency, and accelerate it to a velocity suitable for injection into a drift tube linac.

Introduction

At present, the proposed use of radio-frequency quadrupole (RFQ) structures for the acceleration of low-velocity ions is receiving increased attention. Of special importance is the structure proposed by Kapchinskii and Teplyakov[1] (K-T) which produces strong focusing electric fields which are spatially continuous along the accelerator axis. The longitudinal accelerating fields which are also present are produced by periodic variations of the radius of the pole tips. To produce the required pole tip potentials several RF systems have been proposed. The predominant effort at LASL is to develop the four-vane resonator operating in the TE_{210} mode. Figure 1 shows a schematic view of this type of resonator.

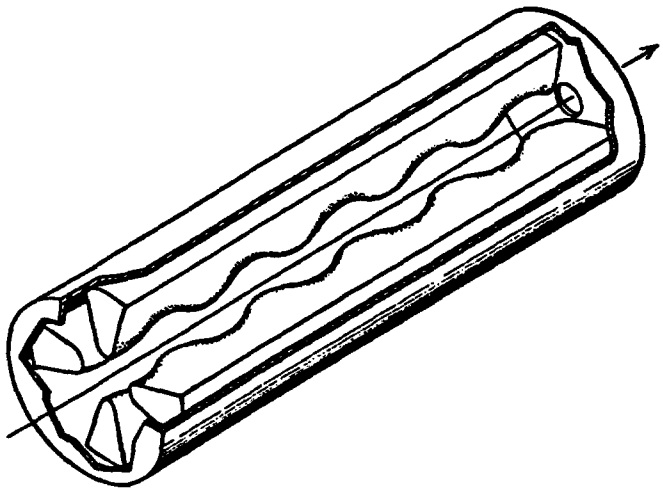

Figure 1.

The expected performance of the RFQ makes it an attractive possibility for use in a variety of accelerator systems. It has been recognized that linac intensity limitations often occur at low velocities where the radial focusing forces from magnetic quadrupoles are weak, and where the longitudinal repulsive forces act for a long time between accelerating gaps. The use of a spatially continuous electric quadrupole force is attractive for the containment of such low-velocity beams. In addition, the longitudinal focusing is greater than in an equivalent drift tube linac for two reasons: (1) for the same frequency the RFQ focusing period is half as long, and (2) for the RFQ the frequency can be higher for a given particle velocity because of the smaller aperture made possible by the strong radial focusing forces.

Beam Dynamics

Our method of calculating RFQ beam dynamics is based on electric field distributions obtained from the lowest order potential function.[1] The coordinate system has been chosen so that the unit cell encompasses an acceleration gap in a symmetrical manner. The unit cell is $\beta_0\lambda/2$ in length, where $\beta_0 c$ is the synchronous velocity. This is shown in Figure 2.

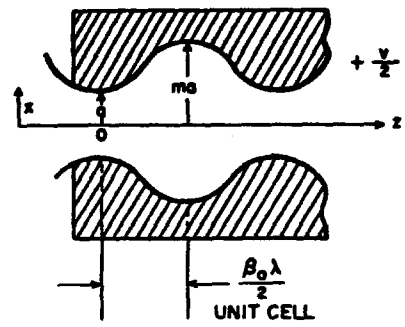

Figure 2.

The electric fields are:

$$E_r = -\frac{XV}{a^2} r\cos 2\psi - \frac{kAV}{2} I_1(kr)\cos kz$$

$$E_\psi = \frac{XV}{a^2} r \sin 2\psi$$

$$E_z = \frac{kAV}{2} I_o(kr)\sin kz$$

where each component is to be multiplied by the time factor $\sin(\omega t + \phi)$. The quantity k equals $2\pi/\beta_0\lambda$, and A and X are given by:

$$A = \frac{m^2 - 1}{m^2 I_o(ka) + I_o(mka)}$$

and

$$X = 1 - A I_o(ka) \quad .$$

Our notation is the same as in Ref. 1 except that our A equals $4/\pi$ times the quantity θ used by K-T. The quantity A, times V the potential difference between vanes, is the change in the axial potential across one unit cell. Therefore, E_o, the average axial field is given by $2AV/\beta_0\lambda$. The quantity X is a measure of the radial focusing strength. It is unity for $m = 1$, and decreases with increasing values of A. For $m = 1.75$ and $ka \ll 1$, both A and X are approximately equal to 0.5.

The hyperbola-like pole tip surfaces[1] which produce the above electric fields in the static approximation are described by the function:

$$x^2 - y^2 = r^2\cos 2\psi = \frac{a^2}{X}\left[\pm 1 - A I_o(kr)\cos kz\right] \quad .$$

In our resonator design we have characterized the pole tip shapes by using two quantities derived from the above equation. One is the pole tip radius which is obtained through a numerical solution. For example, to describe the pole tip radius in the x-z plane, let

0018-9499/79/0600-3469$00.75 © 1979 IEEE

RFQ DEVELOPMENT AT LOS ALAMOS*

T. P. Wangler, K. R. Crandall, and R. H. Stokes, AT-1, MS H817
Los Alamos National Laboratory
Los Alamos, NM 87545

Summary

The basic principles of the radio-frequency quadrupole (RFQ) linac are reviewed and a summary of past and present Los Alamos work is presented. Some beam-dynamics effects, important for RFQ design, are discussed. A design example is shown for xenon and a brief discussion of low-frequency RFQ structures is given.

Introduction

The RFQ is an invention of Kapchinskii and Teplyakov.[1] We can understand RFQ linac operating principles by considering properties of a simple 2D electric quadrupole (Fig. 1). There are four electrodes or poles, charged so that the voltage between adjacent poles is V, and the radial aperture at the pole tip is a. For the static case the potential can be expressed in polar coordinates r and θ as is shown in the figure. If a positive beam is introduced in the central region, it will be focused horizontally and defocused vertically for the polarity shown in Fig. 1. An overall strong focusing in both planes will occur if the polarity is alternated. In the RFQ the polarity is alternated by varying the voltage on the poles sinusoidally in time.

The potential on axis (r=0) in Fig. 1 is zero. To obtain an accelerating field along the quadrupole axis it is necessary to produce a nonzero and spatially varying potential on axis. This can be done by making unequal radial apertures for adjacent pole tips (Fig. 2) where the horizontal apertures are a and the vertical apertures are ma. The potential now consists of the two terms shown in Fig. 2: the quadrupole term, which is reduced by the factor χ, and the term A, which is nonzero on axis. It is easy to show that the sign of this second term is positive when the positive poles have the smaller radial aperture, but is negative when the negative pole apertures are smaller. This suggests that spatially modulated vanes will create a spatially modulated potential on axis, and consequently an accelerating field for particles properly phased.

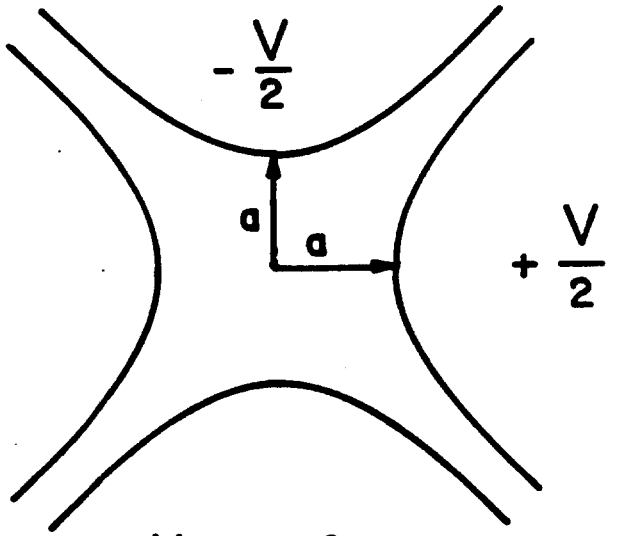

Fig. 1. Cross section of an electric quadrupole with radial aperture a and voltage V between poles. The potential function Φ is given in polar coordinates r and θ.

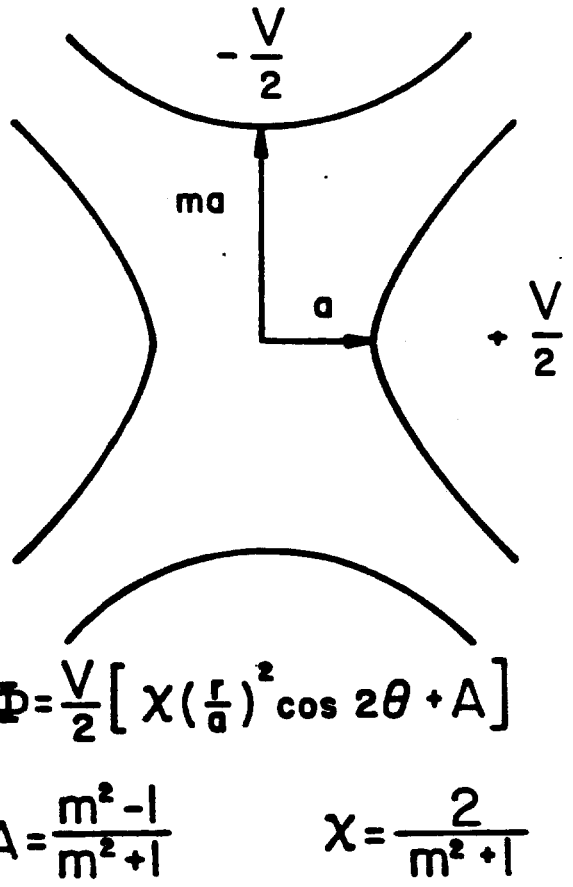

Fig. 2. Cross section of an electric quadrupole with unequal apertures a and am, and voltage V between poles. The potential function Φ is given in polar coordinates r and θ.

*Work supported by the US Department of Energy.

The potential on the axis is generated by moving the poles as above. The accelerating field is given by the gradient of this potential. As βλ becomes large, this field becomes small.

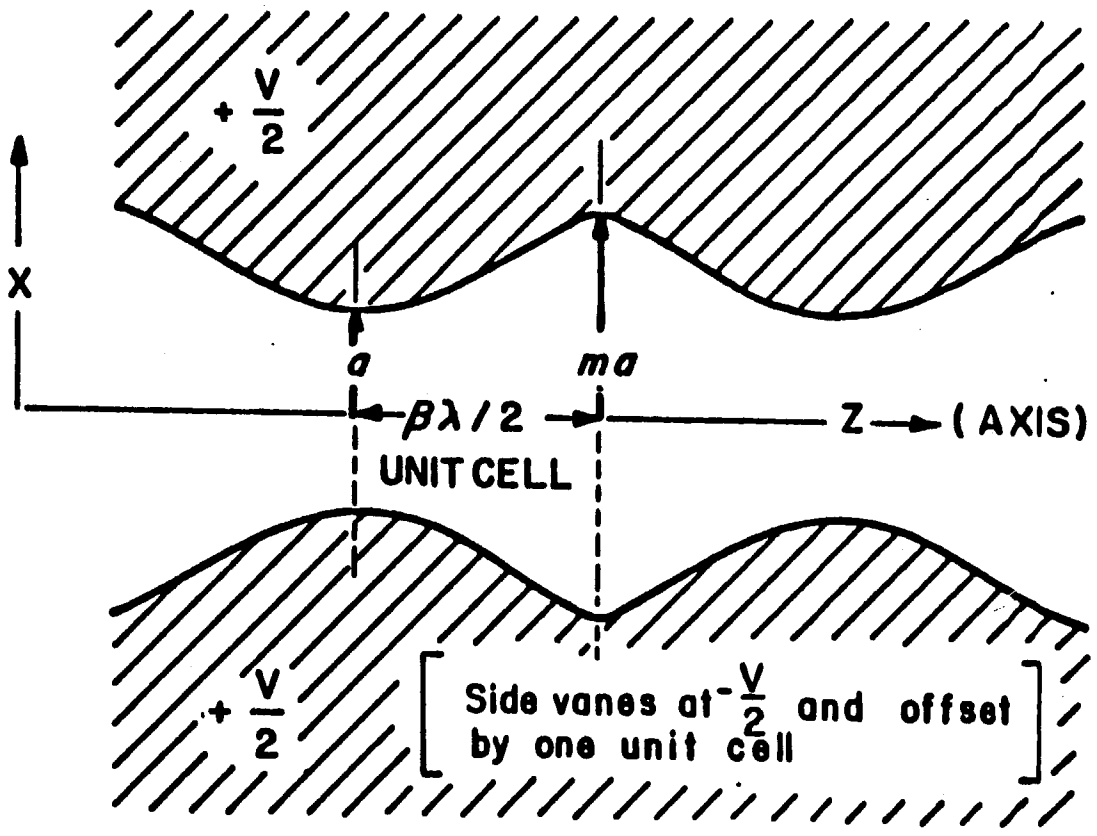
+ V/2
X
a
ma
βλ/2
Z (AXIS)
UNIT CELL
+ V/2
Side vanes at -V/2 and offset by one unit cell

[4] P. Junior et al., ibidem p. 2639
[5] A. Schempp et al., this conference
[6] R.W. Müller et al., this conference
[7] A. Septier, Advances in Electronics and Electron Physics , Academic Press: New York, London, 1961

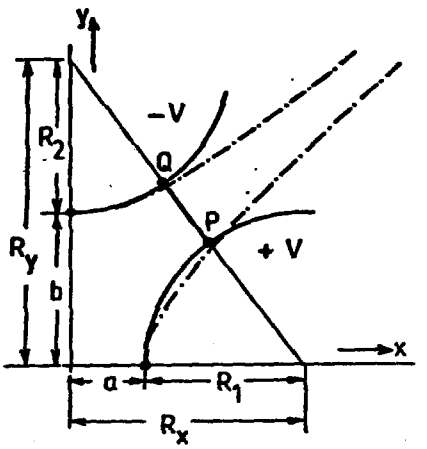

Fig. 1a Transverse cross sections with bore radii R_1 and R_2, dashed hyperbolas correspond to two term case. Note that with types 2 and 3 at constant distance $R_x = R_y$ a larger curvature radius compared to those of the dashed hyperbolas is necessarily involved $R_x = a + b$ usually being taken. In cases 1 and 4 the bore radius agrees with 1.125 a[7]. Peak surface field limitations are not considered.

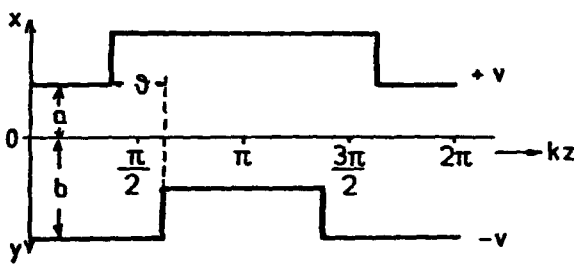

Fig. 1b Longitudinal rectangular cross sections of types 1 and 2

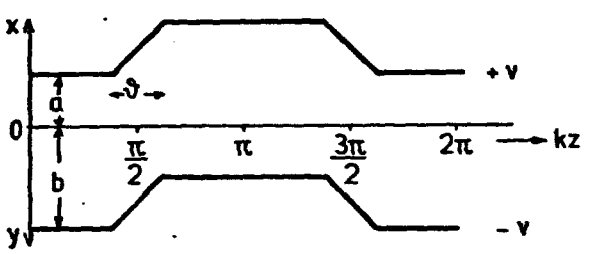

Fig. 1c Longitudinal trapezoidal cross section of type 3

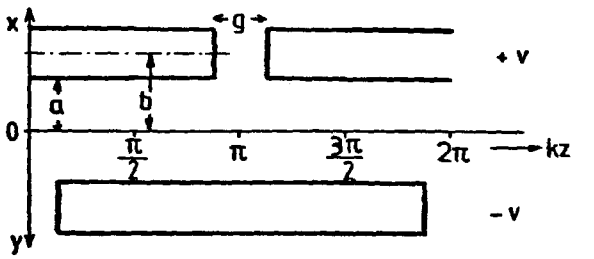

Fig. 1d Longitudinal finger scheme type 4, where acceleration A_{10} is determined by the gap g, lathe required

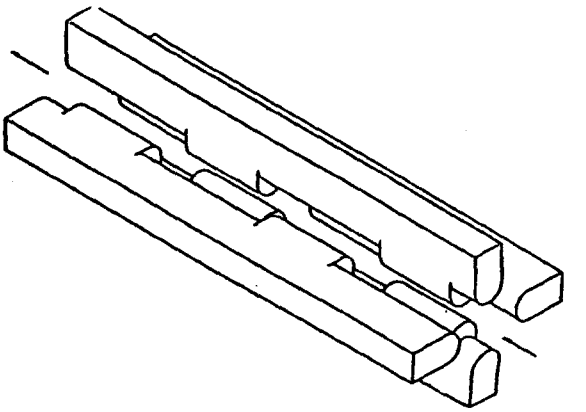

Fig. 2 Sketch of crankshaft, simple milling tool required

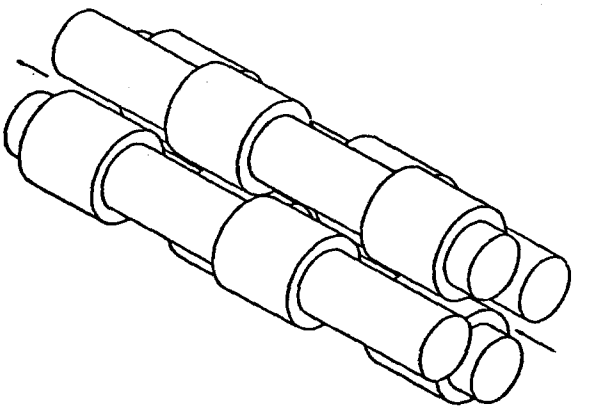

Fig. 3 Sketch of barrels, lathe required

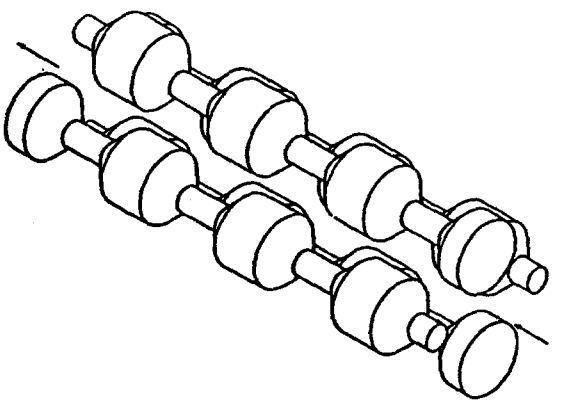

Fig. 4 Sketch of trapezoid, lathe required

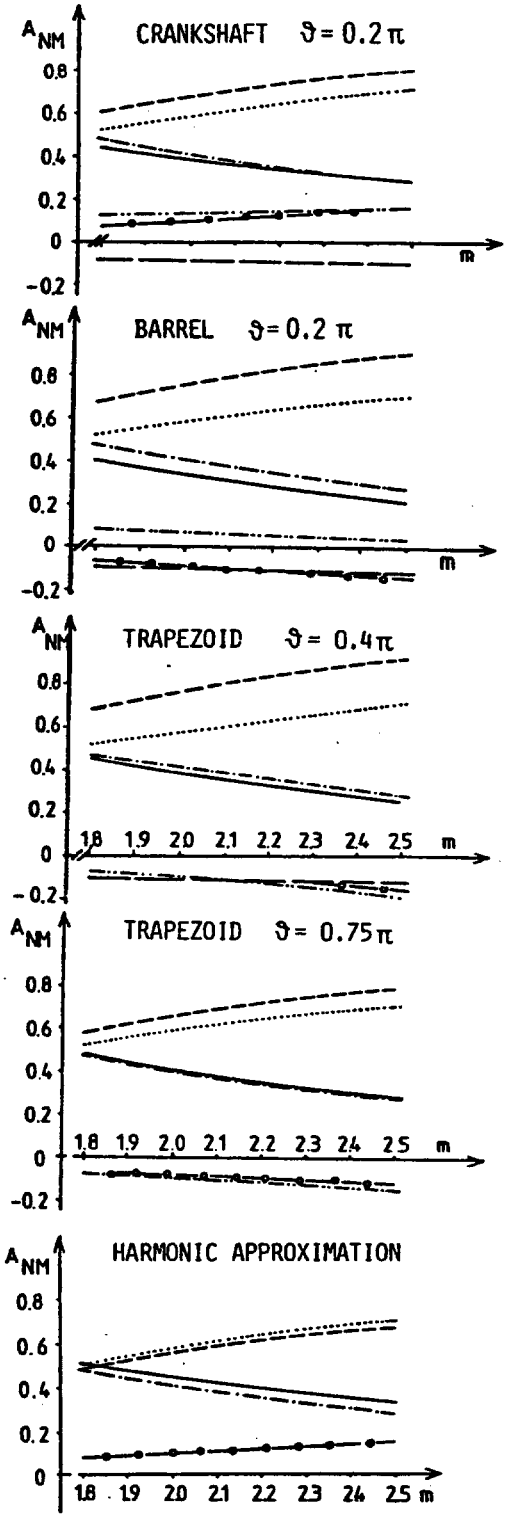

Fig. 5 Field harmonics A_{NM} of representative section with ka = 0.274 versus modulation (a = 3 mm, 108 MHz, 300 keV proton energy)
A_{10}, ideal A_{10}, ideal A_{01}, A_{01}, A_{12}, A_{21}, A_{30}
Normalization $A_{01} = A_{01}/a^2$

$$A_{NM} = A_{NM}/I_{2M}\ (Nk\frac{a+b}{2})$$

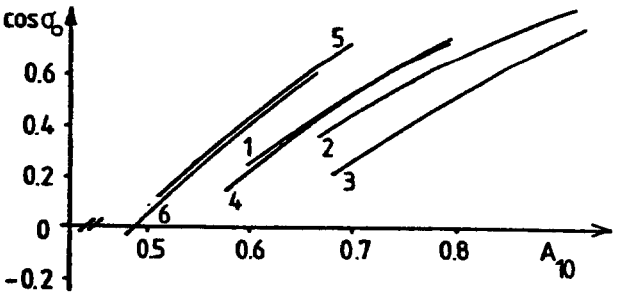

Fig. 6 $\cos\sigma_0$ versus A_{10} of figs. 5, electrode voltage 30 kV
1 crankshaft, 2 barrel, 3 trapezoid $\vartheta = 0.4\pi$, 4 trapezoid $\vartheta = 0.75\pi$, 5 ideal, 6 approximation of 5

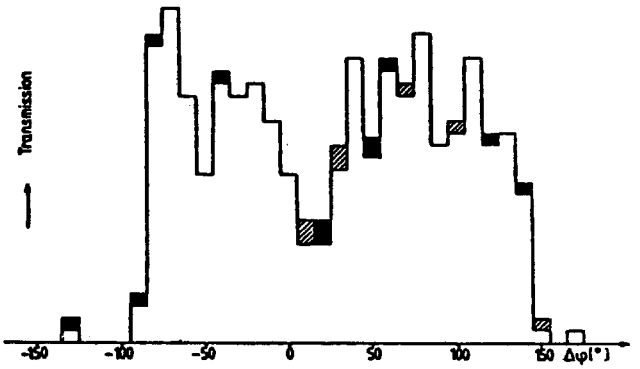

Fig. 7 Gains ■ and losses ▨ of particles due to A_{21} in proton linac[3,4,5]. Transmission about 6 mA, shaper omitted in design, PARMTEQ code, transmission versus phase plotted.

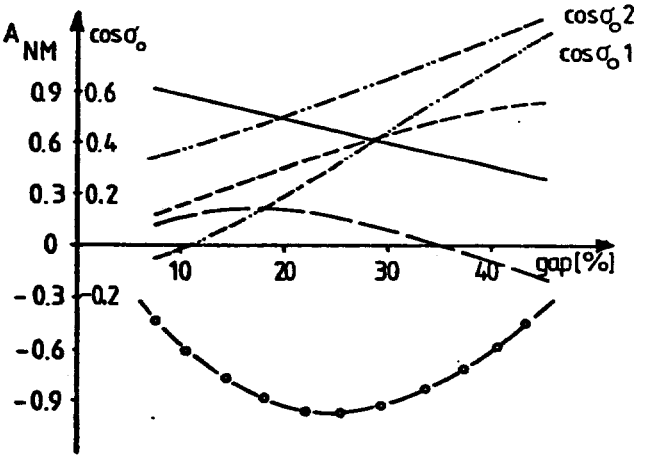

Fig. 8 Field harmonics of fingers type 4 with ka = 0.274 and $\cos\sigma_0$ versus gap in % of $\beta\lambda$, a = 6 mm, 13.5 MHz, 18.75 keV/amu energy, $\cos\sigma_0$ corresponding to
1. 120 kV for ions with ζ/amu = 1/130 resp. 2. 150 kV, 1/208
Legend of curves as in fig. 5

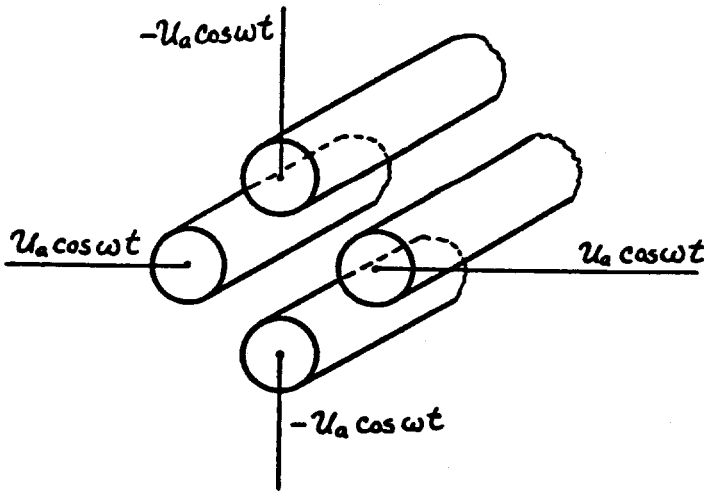

Figure 1.

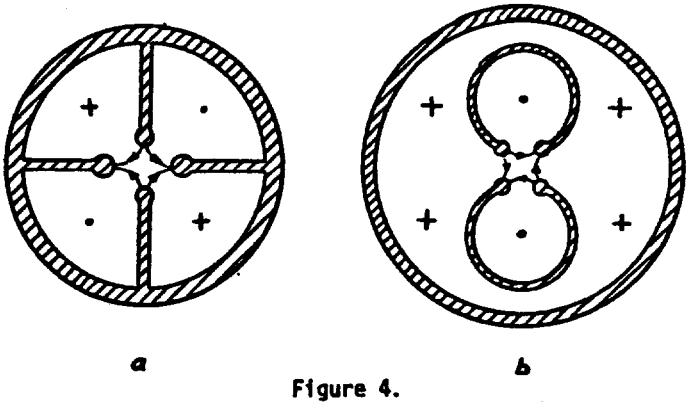

Figure 4.

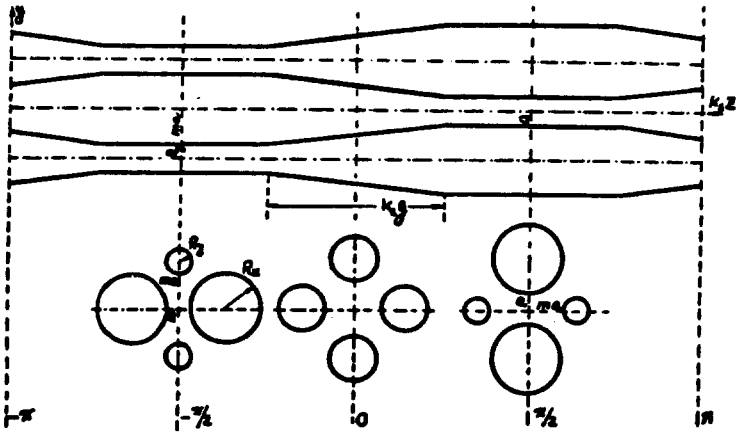

Figure 2.

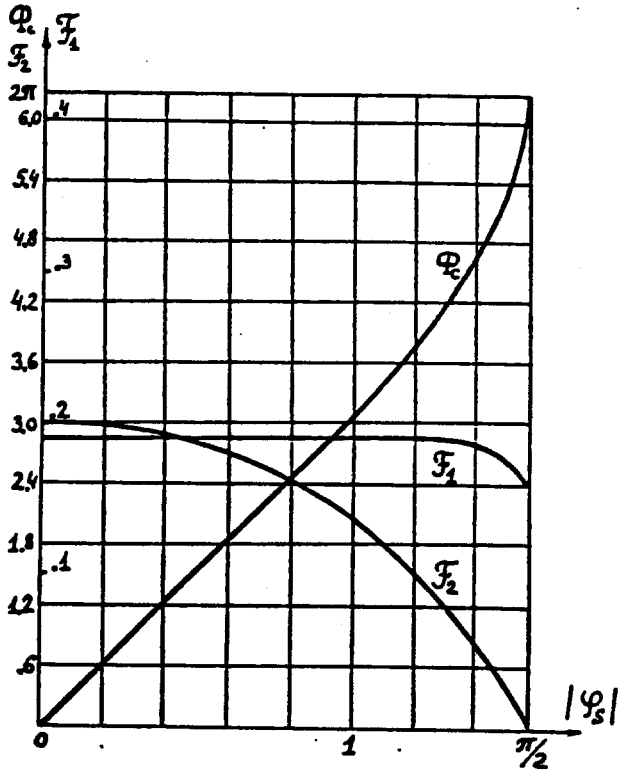

Figure 5.

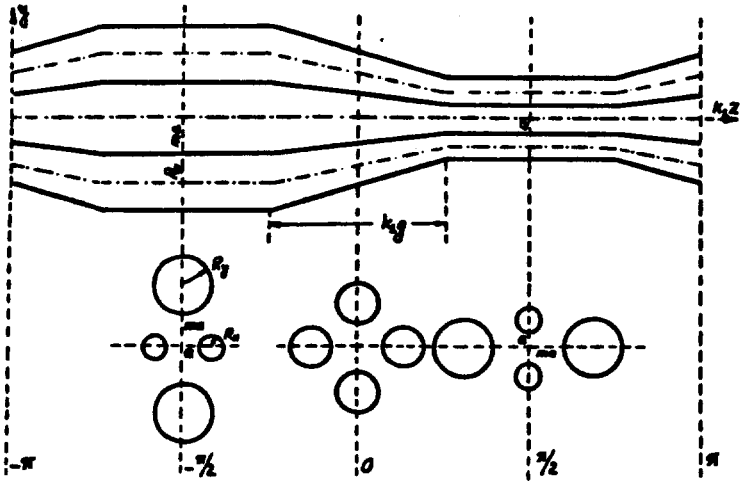

Figure 3.

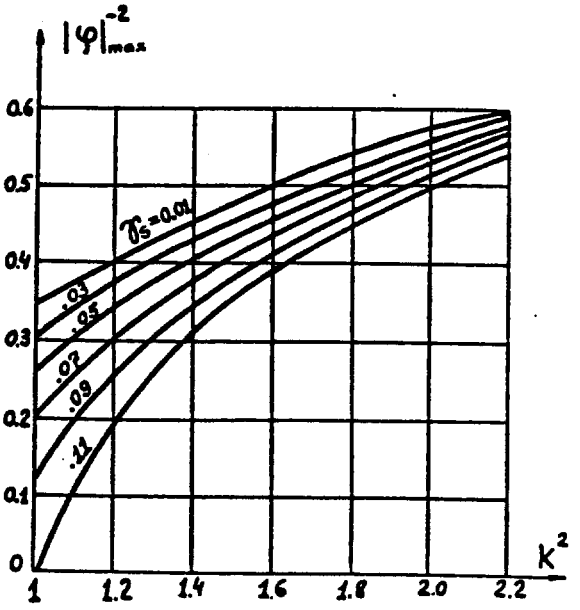

Figure 6.

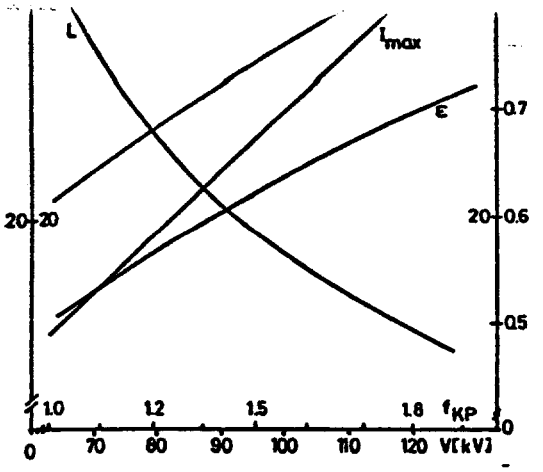

Fig. 3 Optimum beam current limit I_{max}, undepressed phase advance σ_0, undepressed transverse acceptance ε (normalized) and length of gentle buncher versus electrode voltage and Kilpatrick factor

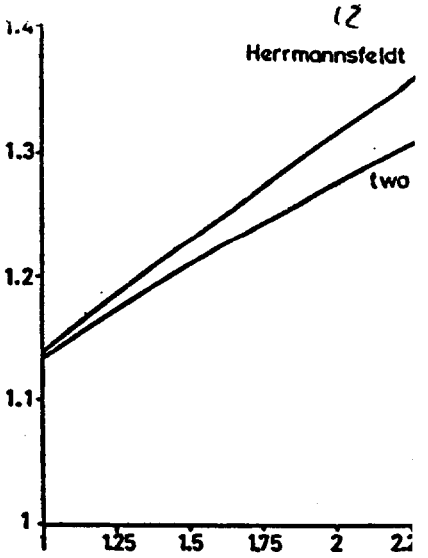

Fig. 5 Field enhancements ver
Curve 1 formula for tw
curve 2 exact calculat

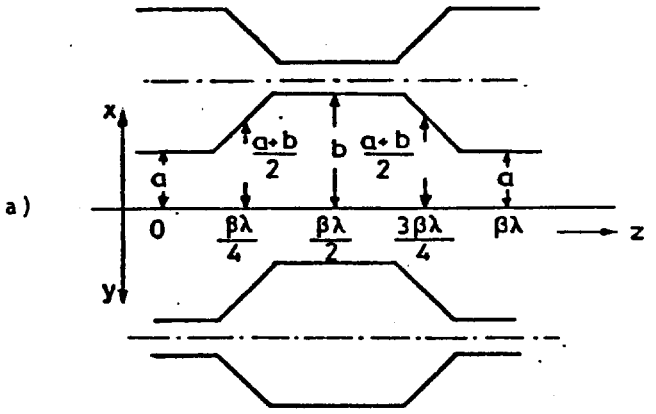

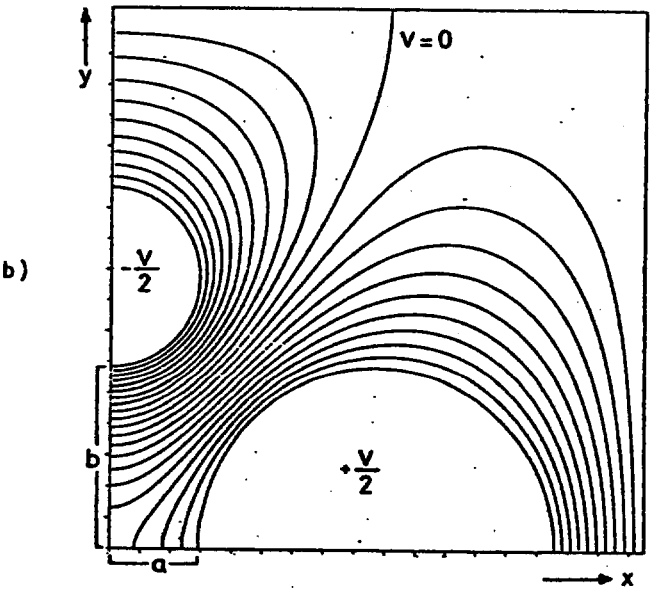

Fig. 4 Cross sections of electrodes
a) longitudinal scheme
b) transverse scheme and potential distribution calculated with the Herrmannsfeldt code[14] at z = 0 in the case of modulation 2

Π Mode DT + Cone RFQ

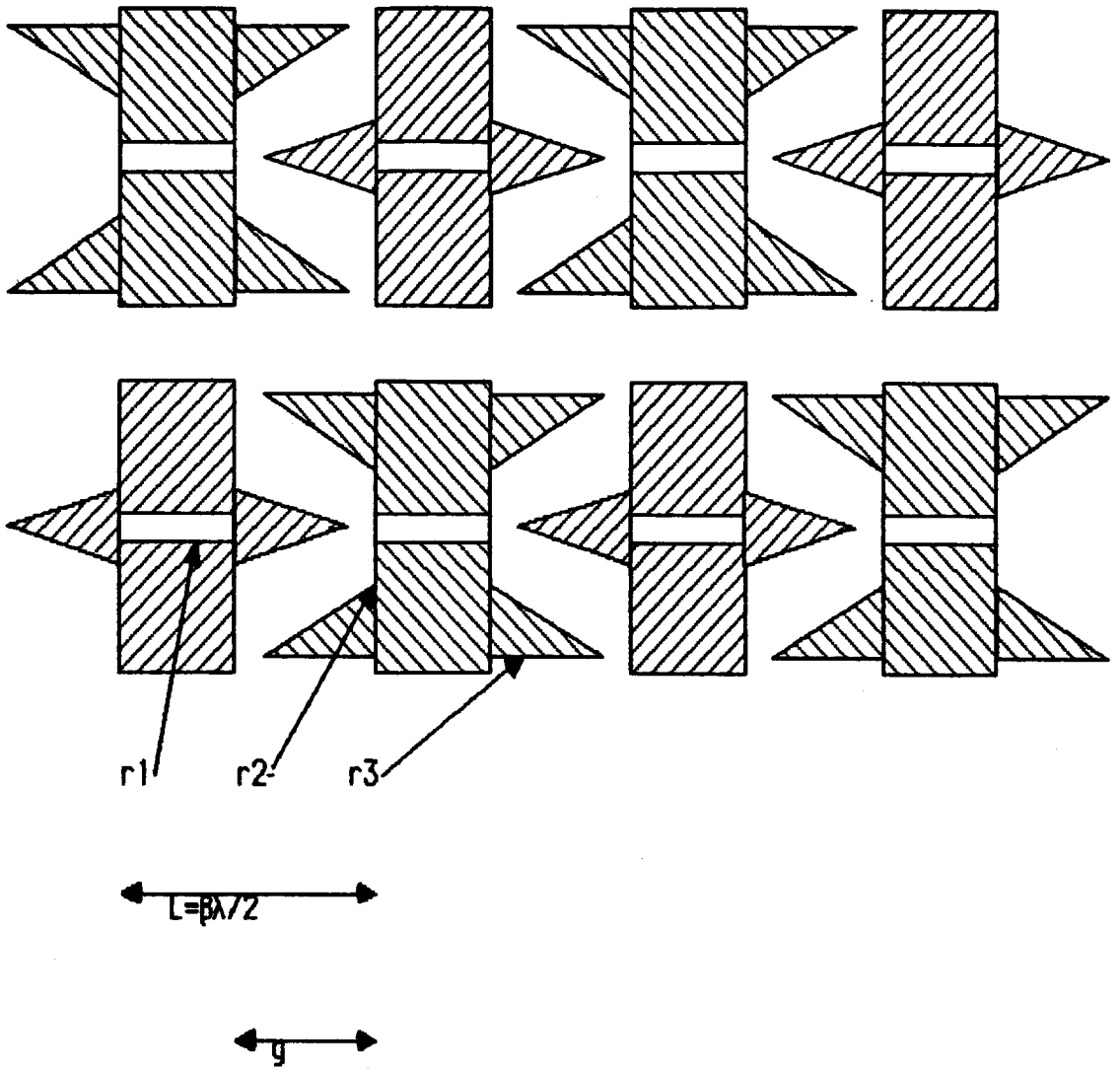

Solve for Fields in Gap Region, find radii a,b of cones as function of z.

$$\Psi = AI_0(kr)\sin(kz) + Br^2\cos(2\phi)$$

k is <u>not</u> related to $\beta\lambda/2$, can be chosen. Potentials $\pm V/2$ on drift tubes and cones.

Find

$$A = V/[2\sin(kg/2)I_0(kr_1)]$$

$$B = V[2+(I_0(kr_3)-I_0(kr_2))/I_0(kr_1)]/2(r_3^2+r_2^2)$$

$$2Ba^2 = V\{1-[I_0(ka)/I_0(kr_1)][\sin(kz)/\sin(kg/2)]\}$$

Then the cone radius is determined as a fcn. of z.

Energy gain

Get E_z, calculate the energy gained in a half cell of length $\beta\lambda/2$. ($\Psi \alpha \cos(\omega t - \phi)$)

$$\Delta E = T\, eV \cos\phi$$

$$T = \frac{[\cos(\pi g/\beta\lambda) + (2\pi/k\beta\lambda)\cot(kg/2)\sin(\pi g/\beta\lambda)]}{1 - (2\pi/\beta\lambda k)^2}$$

In order to get a good Transit time factor, the {horn / cone} structure is alternated with a short gap without "horns". (I. M. Kapchinsky, 1980, 1985) This gives strong focussing in the horn region, poor acceleration; but good acceleration, net defocussing in the short gap region. In UNAL-IS, the second tank gave 16-2 Meo/8.7 m which is as high as the gradient in our Tank I.